Appl Magn Reson (2014) 45:623–640
DOI 10.1007/s00723-014-0542-6

Applied
Magnetic Resonance

Incommensurate Phases of the $MgSiF_6{\cdot}6H_2O$ Crystals: EPR and Group-Theoretical Studies

Peter G. Skrylnik · Albert M. Ziatdinov

Received: 21 March 2014 / Revised: 29 April 2014 / Published online: 24 May 2014

Abstract The group-theoretical study of the structural phase transition to incommensurate state of $MgSiF_6{\cdot}6H_2O$ crystals, revealed by the electron paramagnetic resonance (EPR) method, as well as analysis of the EPR results, are presented. The consideration of temperature dependences of Mn^{2+} admixture ion EPR spectrum symmetry and parameters leads to the conclusion that at $T_{i1} = 370 \pm 0.3$ K they undergo second-order structural phase transition to incommensurately modulated state, the order parameter of this transition may be the angle of $[Mg(H_2O)_6]^{2+}$ octahedra rotation around crystal $\mathbf{C}_3$ axis. At temperature decreasing below T_{i1} the gradual transformation of plane-wave modulation of lattice displacements into soliton mode occurs, which is interrupted by the first-order phase transition at $T_{i2} = 343 \pm 0.3$ K accompanied by abrupt decrease in modulation amplitude. At $T_c = 298.5 \pm 0.3$ K the first-order improper ferroelastic phase transition into monoclinic phase occurs. The group-theoretical analysis of the phase transition at T_{i1} in the investigated crystals, carried out for the first time, has shown that the existence of the incommensurately modulated phase is conditioned by the fundamental reasons (presence of Lifshitz invariant). The conclusions of this analysis on the nature of order parameter, the structural motifs of incommensurate phase and the possible character of temperature evolution of the structure are in agreement with the EPR investigation data.

1 Introduction

Magnesium hexafluorosilicate hexahydrate ($MgSiF_6{\cdot}6H_2O$) belongs to the large family of the $ABX_6{\cdot}6H_2O$ (where A is a divalent metal, B tetravalent element and X

P. G. Skrylnik · A. M. Ziatdinov (✉)
Institute of Chemistry of the Far Eastern Branch of the Russian Academy of Sciences,
159, Prospekt 100-letiya, 690022 Vladivostok, Russia
e-mail: ziatdinov@ich.dvo.ru

halogen) crystals. Crystals of this family are characterized by rhombohedrally distorted CsCl-type lattice consisting of trigonally distorted octahedra of $[A(H_2O)_6]^{2+}$ and $[BX_6]^{2-}$ groups, connected via hydrogen bonds; the octahedra may be distributed between two orientations with different rotations around the trigonal axis ($\mathbf{C}_3$) of crystals [1–6]. The interest attracted by these compounds is accounted for by that, despite the same crystal structure motif and similar lattice parameters, some crystals of the family undergo structural phase transitions [2–19], and others preserve symmetry down to low temperature [2, 20–22]. At present there is no single point of view on the mechanisms of the phase transitions in these crystals, there exist ambiguities in their symmetry at room and higher temperature.

In the $MgSiF_6{\cdot}6H_2O$ crystals using X-ray diffraction Syoyama and Osaki [8] have discovered improper ferroelastic phase transition at $T_c \approx 299$ K, which is characterized by the reduction of symmetry from high-temperature rhombohedral space group $R\bar{3}m$ down to low-temperature monoclinic space group $P2_1/c$. Later this transition has been confirmed by the calorimetric studies by Weir et al. [23]. The structure of the phase below T_c [8] has been corroborated by Jehanno and Varret [4], Chevrier and Jehanno [5] and Cherkasova et al. [24]. However, above T_c, according to the results of papers [4, 5], this crystal belongs to space group $P\bar{3}$ and its structure may be presented as the sequence of alternating domains of two types, forming layers being parallel to the pseudohexagonal plane, each contains two orientations of the octahedra of $[Mg(H_2O)_6]^{2+}$ and $[SiF_6]^{2-}$. The result is the periodic antiphase structure built of ordered low-temperature monoclinic ($P2_1/c$) unit cells with integer period. For $Mg_{1-x}Fe_xSiF_6{\cdot}6D_2O$ [25] and $MgSiF_6{\cdot}6D_2O$ [26] crystals above T_c Chevrier pointed out space group $P\bar{3}$ as well. However, as indicated in Inorganic Crystal Structure Database (ICSD [27]) and Landolt-Boernstein handbook [28], the obtained data should be interpreted within the framework of space group $R\bar{3}$ instead of $P\bar{3}$. Therefore, at present there exist divergences in the interpretations of diffraction data for $MgSiF_6{\cdot}6H_2O$ crystals above T_c, and consequently, there is uncertainty in symmetry and structure of the crystals for those temperatures.

In this paper the results of electron paramagnetic resonance (EPR) investigations of the $MgSiF_6{\cdot}6H_2O{:}Mn^{2+}$ crystals are reported and discussed, making an emphasis on structural phase transitions above T_c and 'intermediate' phase between high-temperature axial phase and low-temperature monoclinic one, which have features specific for the incommensurate structural states [14, 15]. The results of group-theoretical analysis of possible paths of the phase transitions from high-temperature axial phase are presented as well, which point out the possibility of realization of the structurally incommensurate states and provide the explanation for observed peculiarities of the Mn^{2+} EPR spectra on the basis of symmetry consideration.

2 Experimental

Single crystals of $MgSiF_6{\cdot}6H_2O$ doped with natural abundance of Mn^{2+} ions have been grown from the aqueous solution of commercial magnesium hexafluorosilicate at room temperature. The $\mathbf{C}_3$-axis in most of the samples was readily determined by inspection and then it was identified as the [111] direction in cubic coordinates.

The EPR spectra have been measured using X-band spectrometer Bruker EMX-6/1 (production of Germany), and Q-band spectrometer RE-1308 (production of Russia) in three mutually perpendicular crystal planes. The orientation of single crystal with respect to the external constant magnetic field $\boldsymbol{B}_0$ direction was varied with two-axis goniometer system. The temperature range of experiments was from 100 to 380 K. The crystal temperature was varied by changing the temperature of gaseous nitrogen flow passing through the quartz Dewar tube containing the crystal investigated. To monitor temperature the copper–constantan thermocouples with base point at the ice melting temperature have been used. The accuracy of monitoring and stability of temperature was $\approx$0.3 K and $\approx$0.1 K/h, respectively.

3 Results

At temperature above $T_{i1} = 370 \pm 0.3$ K the EPR spectrum of the $MgSiF_6{\cdot}6H_2O{:}Mn^{2+}$ crystals is axial with $\mathbf{z}\|\mathbf{C}_3$. When the external constant magnetic field $\boldsymbol{B}_0$ is along $\mathbf{C}_3$ the spectrum consists of 5 × 6 hyperfine structure (HFS) lines of Mn^{2+} ($3d^5$, $S = 5/2$, $I = 5/2$). As the angle between $\boldsymbol{B}_0$ and $\mathbf{C}_3$ (polar θ angle) tends to 'magic' value ($54^\circ 44'$) the width of HFS lines increases. At any θ angle value the shapes and widths of HFS lines do not change at rotating the crystal around $\mathbf{C}_3$ axis (at varying azimuthal ϕ angle). This fact points out the absence of disorientation of the cubic crystal field axes on different Mn^{2+} ions around $\mathbf{C}_3$ [29], i.e., the observed spectrum corresponds to one type of Mn^{2+} centers. It is described by conventional axial spin Hamiltonian with the following parameters (at $T = 372$ K): $g_\perp \cong g_\| = 2.0009 \pm 0.0003$, $D = (-258 \pm 1) \times 10^{-4}$ cm^{-1}, $a = (8 \pm 0.5) \times 10^{-4}$ cm^{-1}, $A_\perp \cong A_\| = (-90 \pm 0.5) \times 10^{-4}$ cm^{-1}. Such EPR spectrum is typical of admixture Mn^{2+} ions substituting A^{2+} positions (in the centers of symmetry of water octahedra) in rhombohedral phase of the $ABX_6{\cdot}6H_2O$ crystals [9, 22, 30, 31].

At decreasing temperature below T_{i1} the HFS lines, excluding central line set corresponding to the transitions $|S_z = 1/2, I_z = m\rangle \leftrightarrow |S_z = -1/2, I_z = m\rangle$, at first broaden and then gradually transform to the two-peak form with spectral continuum between peaks (Fig. 1; for detailed lineshape analysis the low-field HFS line with maximal splitting corresponding to the transition $|S_z = 5/2, I_z = 5/2\rangle \leftrightarrow |S_z = 3/2, I_z = 5/2\rangle$ has been chosen). However, despite the mentioned transformation of HFS lineshape below T_{i1}, symmetry of the Mn^{2+} EPR spectrum and direction of its principal axis remain the same. Increasing temperature results in reversed spectrum evolution. Temperature T_{i1} of the transition from one type of spectrum to another does not depend on the direction of temperature varying, microwave frequency, orientation of $\boldsymbol{B}_0$ with respect to $\mathbf{C}_3$ and chosen HFS line. All these facts are the evidences that T_{i1} is the temperature of the second-order phase transition (not the temperature of dynamic averaging the structurally inequivalent positions of complex ions in the EPR timescale).

At $T_{i2} = 343 \pm 0.3$ K (when cooling) the step-wise changes of the EPR line parameters as well as HFS lineshapes (Fig. 2) with temperature hysteresis $\approx$1 K have been observed. Below T_{i2} the HFS line may be presented as two distinct components of different widths without spectral continuum between them (Fig. 3).

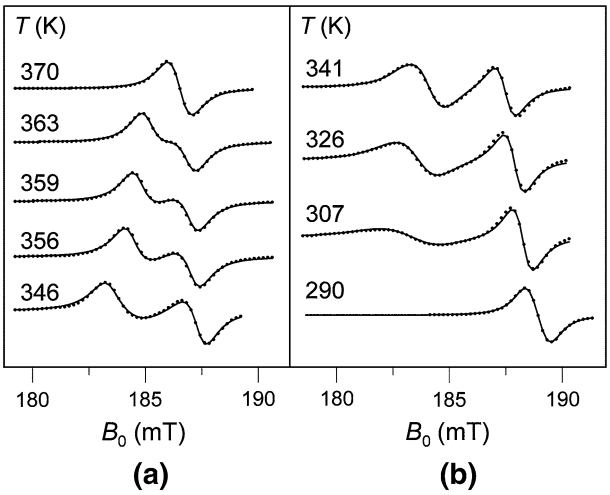

Fig. 1 Temperature evolution of the Mn^{2+} EPR low-field HFS line for $MgSiF_6{\cdot}6H_2O{:}Mn^{2+}$ crystals at X-band and $\boldsymbol{B}_0 \| \mathbf{C}_3$. *Dotted* and *solid lines* correspond to experimental and theoretical spectra, respectively: **a** $T > T_{i2}$ (calculations within the framework of the model of incommensurate phase), **b** $T < T_{i2}$ (calculations as sum of distinct components)

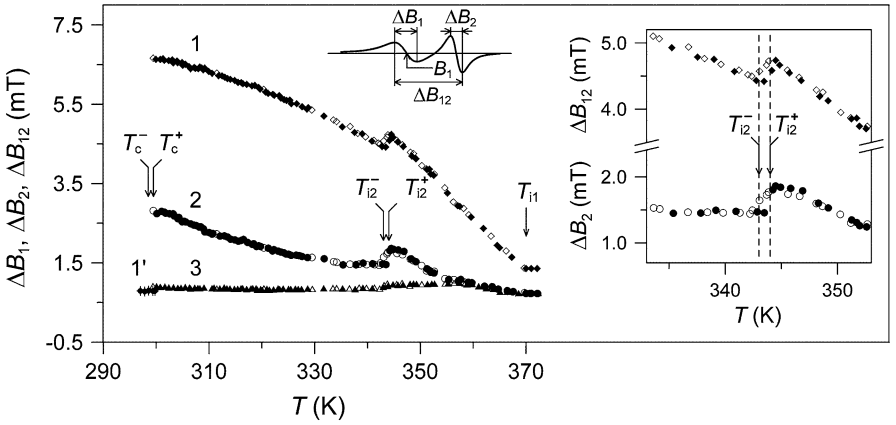

Fig. 2 Temperature dependences of the Mn^{2+} EPR low-field HFS lineshape parameters for $MgSiF_6{\cdot}6H_2O{:}Mn^{2+}$ crystals. *1* ΔB_{12}, *1′* line width in ferroelastic phase, *2* ΔB_1, *3* ΔB_2. The *black* and *white dots* refer to parameters at heating and cooling of the crystals, respectively. Definitions of the studied lineshape parameters are presented too. Inset presents the temperature region around T_{i2} in details. Q-band, $\boldsymbol{B}_0 \| \mathbf{C}_3$

At decreasing temperature below T_{i2} the low-field component of the HFS line broadens, whereas the width of the high-field component remains almost invariable (Fig. 2). However, despite substantial changes in the shapes of spectral lines below T_{i2}, symmetry and direction of the principal axis of EPR spectrum remain unchangeable at that transition too.

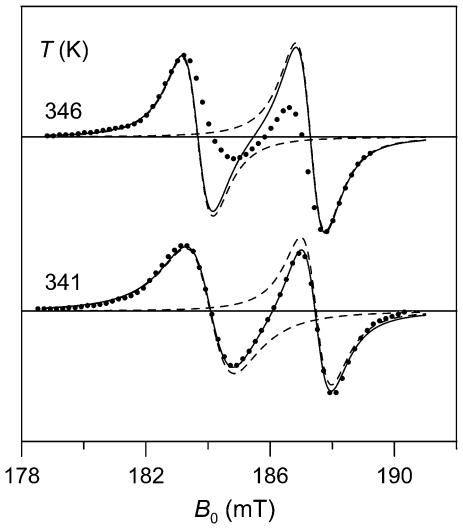

Fig. 3 Experimental Mn^{2+} EPR low-field HFS lineshapes at $T = 346$ K ($>T_{i2}$) and $T = 341$ K ($<T_{i2}$) and their approximations by two Lorentzians. *Dots*, *dashed* and *solid lines* correspond to experimental spectra, components of the approximation and results of approximation, respectively. X-band, $\boldsymbol{B}_0 \| \mathbf{C}_3$

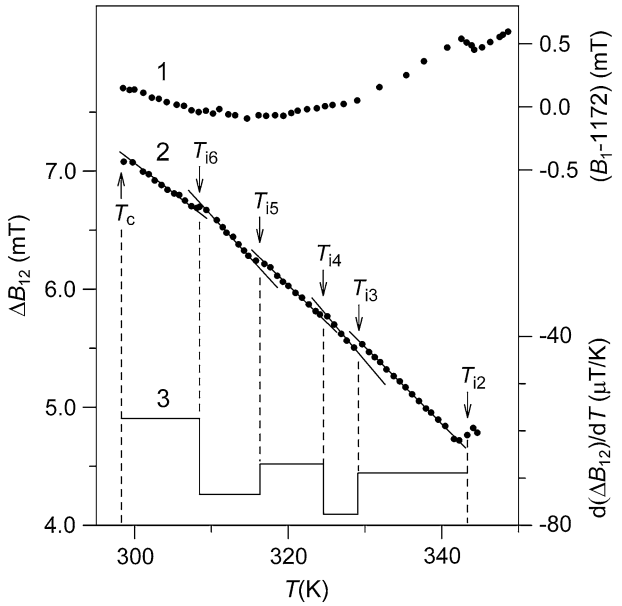

Fig. 4 Temperature dependence of the Mn^{2+} EPR low-field HFS lineshape parameter B_1 (*1*), ΔB_{12} (*2*) and that of the slope $d(\Delta B_{12})/dT$ (*3*) for $MgSiF_6{\cdot}6H_2O{:}Mn^{2+}$ crystals. The temperatures of the step-wise changes in the slope of the $\Delta B_{12}(T)$ are designated as T_{in} ($n = 2$–6). $\boldsymbol{B}_0 \| \mathbf{C}_3$ (*1* Q-band; *2*, *3* X-band)

Further decreasing temperature below T_{i2} leads to the sequence of step-wise changes in the slopes of temperature dependences of the HFS lineshape parameters (for instance, B_1 and ΔB_{12}) and discontinuities in the parameters themselves, though they are significantly less than those at T_{i2} (Fig. 4). These peculiarities occur at

almost identical values of the lineshape parameters, while their temperature values T_{in} ($n = 2$–6) vary from sample to sample within ≈ 4 K.

As temperature decreases below $T_c = 298.5 \pm 0.3$ K, the crystals undergo the first-order phase transition to monoclinic phase with temperature hysteresis ≈ 1 K. At these temperatures the EPR spectrum corresponds to six spatially inequivalent rhombic Mn^{2+} centers, **z**-axis of each center is deviated from $\mathbf{C}_3$ axis by angle $(8 \pm 2)°$. Angular dependences of EPR spectra for all spatially inequivalent Mn^{2+} centers are well described by conventional rhombic spin Hamiltonian with parameters (at $T = 290$ K) as follows: $g_\perp \cong g_\parallel = 2.0010 \pm 0.0005$, $D = (-275 \pm 2) \times 10^{-4}$ cm^{-1}, $|E| = (30 \pm 5) \times 10^{-4}$ cm^{-1}, $a = (8 \pm 2) \times 10^{-4}$ cm^{-1}, $A_\perp \cong A_\parallel = (-92 \pm 1) \times 10^{-4}$ cm^{-1}. For the orientation $\boldsymbol{B}_0 \| \mathbf{C}_3$, the position and width of the Mn^{2+} HFS line immediately after phase transition are approximately the same as those of the narrow component of the Mn^{2+} HFS line in the inhomogeneous phase immediately before phase transition (Figs. 1, 2).

Analysis of the $MgSiF_6{\cdot}6H_2O{:}Mn^{2+}$ EPR angular dependences and variation of the relative intensities of spectra from inequivalent EPR centers (from sample to sample and from experiment to experiment for given sample) as well as studying these crystals with polarization microscope show that below T_c considered crystal consists of orientational domains of three kinds, connected with each other by 120° rotation around $\mathbf{C}_3$ axis and each domain contains two types of spatially inequivalent Mn^{2+} centers. It follows from these facts that $MgSiF_6{\cdot}6H_2O$ crystal is improper ferroelastic below T_c. The number of Mn^{2+} centers within domain and symmetry of EPR spectrum of certain paramagnetic ion in the $MgSiF_6{\cdot}6H_2O{:}Mn^{2+}$ crystals at $T < T_c$ are in agreement with the data of structural investigations at the mentioned temperatures [4, 5, 8, 25].

Within the temperature range from T_{i1} to T_c at varying angle ϕ (at $\theta \neq 0°, 90°$), the angular dependence of the HFS lineshape with 120° period has been observed (Fig. 5). The amplitude of mentioned angular changes of HFS lineshape parameters increases as temperature decreases (Fig. 5). For temperature ranging from T_{i2} to T_c while angle θ tends to the 'magic' value the HFS line components approach each other and completely merge at indicated value (Fig. 6). At that the width of the low-field broad component of HFS line decreases while that of high-field narrow component increases (Fig. 6, inset).

4 Analysis of experimental data

The presence of two edge singularities with spectral continuum between them for all HFS lines (excepting central set) of the $MgSiF_6{\cdot}6H_2O{:}Mn^{2+}$ EPR spectrum from T_{i1} to T_{i2} (Fig. 1) gives evidence for non-random variation of the resonance magnetic field B_r on Mn^{2+} ions throughout the sample [32]. The absence of such peculiarities for the HFS lines of central set (whose positions in the first approximation do not depend on fine structure parameter D) allows to conclude that the reason for B_r spread is the variation of D, not the HFS parameter A, values for different Mn^{2+} ions. Since for the Mn^{2+} EPR spectrum the non-zero value of D testifies the trigonal distortion of water octahedra [33], then non-random spread of this parameter results

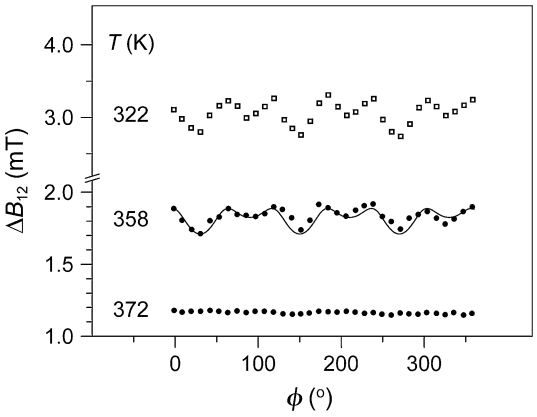

Fig. 5 Angular dependences of the value of Mn^{2+} EPR low-field HFS ΔB_{12} parameter for $MgSiF_6{\cdot}6H_2O{:}Mn^{2+}$ crystals at rotating the sample around the $\mathbf{C}_3$ axis (along the ϕ angle), which makes the angle $\theta \approx 50^{\circ}$ with $\boldsymbol{B}_0$, at different temperatures (the X-band). *Dots* correspond to experimental values. *Solid line* corresponds to the theoretical angular dependence (describing the experimental one for $T = 358$ K), calculated in the framework of the model of quadratic modulation of D: $\delta D = d{\cdot}\phi^2$, $\phi(z) = \delta\phi{\cdot}\cos(z)$ with $\delta\phi = 7.1^{\circ}$, $d = 0.108 \times 10^{-4}$ $cm^{-1}/(degree)^2$

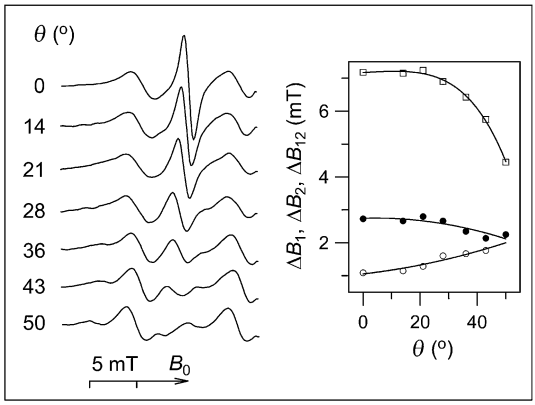

Fig. 6 Angular dependences of the Mn^{2+} EPR low-field HFS lineshape for $MgSiF_6{\cdot}6H_2O{:}Mn^{2+}$ crystal at the θ angle rotation. The *full circles*, *open circles* and *squares* in *inset* correspond to ΔB_1, ΔB_2 and ΔB_{12} values, respectively (*lines* are presented only as guides for the eye). Definitions of all mentioned lineshape parameters are presented in Fig. 2. The X-band, $T = 328$ K

in the conclusion on the non-random variation of the trigonal distortions of water octahedra in the inhomogeneous phase of the considered crystals.

The HFS lineshape of the $MgSiF_6{\cdot}6H_2O{:}Mn^{2+}$ EPR spectrum observed below T_{i1} and the character of its temperature evolution are well known [32] to be inherent for systems with one-dimensional incommensurate (or long-period) modulation of lattice displacements. In such systems resonance field B_r on the certain paramagnetic center is a function of small lattice displacements $u(z)$ modulated along $\mathbf{z}$ direction with period being incommensurate with the unmodulated lattice period: $u(z) = A(z){\cdot}\cos\varphi(z)$, where $A(z)$ and $\varphi(z)$ are amplitude and phase of the modulation wave along $\mathbf{z}$ direction, respectively. In general, B_r may be expanded into series in $u(z)$ [32]:

$$B_r = B_{r0} + b_1 \cos[\phi(z)] + b_2 \cos^2[\phi(z)] + \cdots, \quad (1)$$

where B_{r0} is the resonance field value in the absence of modulation distortions, b_i—some constants (neglecting amplitude modulation of the lattice displacement wave). Resulting HFS lineshape for the incommensurate phase of the crystals may be simulated by integration on possible B_r values with using some single lineshape (Lorentzian, in most cases), i.e., by convolution.

The appearance of the Mn^{2+} EPR HFS lineshape dependence on angle ϕ below T_{i1} (Fig. 5) and increase in its amplitude at decreasing temperature are evidences for the appearance of disorientation of the cubic crystal field axes on Mn^{2+} ions (rotations of the water octahedra around $\mathbf{C}_3$ axis by different angles with respect to their positions in trigonal phase above T_{i1}) below that temperature and for increasing amplitude of such disorientation at decreasing temperature, respectively. Obviously, water octahedra disorientation revealed below T_{i1} may be caused by modulation of their rotations around $\mathbf{C}_3$ axis with respect to their positions in high-temperature trigonal phase. Therefore, in the inhomogeneous phase of $MgSiF_6{\cdot}6H_2O{:}Mn^{2+}$ crystals both axial distortion of water octahedra and angle of their rotations around $\mathbf{C}_3$ axis with respect to their positions in high-temperature trigonal phase are candidates for the role of primary order parameter of the phase transition to incommensurate phase (i.e., characteristic lattice distortion arising at transition). However, the presence of two types of $[Mg(H_2O)_6]^{2+}$ complexes, rotated around $\mathbf{C}_3$ axis by certain angle $\Delta\phi$ relative to each other (but with equal distortion along **z**-axis of complex, i.e., with equal D values), within each orientational domain in monoclinic phase of the $MgSiF_6{\cdot}6H_2O$ crystals [4, 5, 8], testifies that primary lattice distortion, arising at the transition to incommensurate phase, is the angle of water octahedra rotation around $\mathbf{C}_3$ axis relative to their positions in high-temperature trigonal phase (Fig. 7).

Axial distortion of the water octahedra (and, therefore, D), as far as structure possesses inversion center, should be proportional to an expansion in even powers of primary angle of rotation around $\mathbf{C}_3$ axis [34]. Dependence of D value on octahedra trigonal distortion may be considered as linear one for small distortions [33]. Taking these facts into account, at $\boldsymbol{B}_0 \| \mathbf{C}_3$ in the Eq. (1) the odd power terms in $\cos\varphi$ may be neglected.

The calculations of HFS lineshapes from T_{i1} to $\approx(T_{i1} - 10$ K), conducted with only even terms retained in Eq. (1), have demonstrated that experimental lineshapes may be successfully described in the approximation of linear $\varphi(z)$ dependence, i.e., in plane-wave regime of D modulation (Fig. 1). Evidently, the possibility of such description of the HFS lineshapes testifies to the plane-wave modulation of trigonal distortions in the crystals at mentioned temperatures as well.

At $T \to T_{i1}$ the HFS lineshape becomes symmetrical and, as a consequence, experimental spectra near T_{i1} may be fitted with good accuracy taking into account only quadratic modulation term depending on temperature according to the power law:

$$b_2(T) = a(T_{i1} - T)^{2\beta}, \quad (2)$$

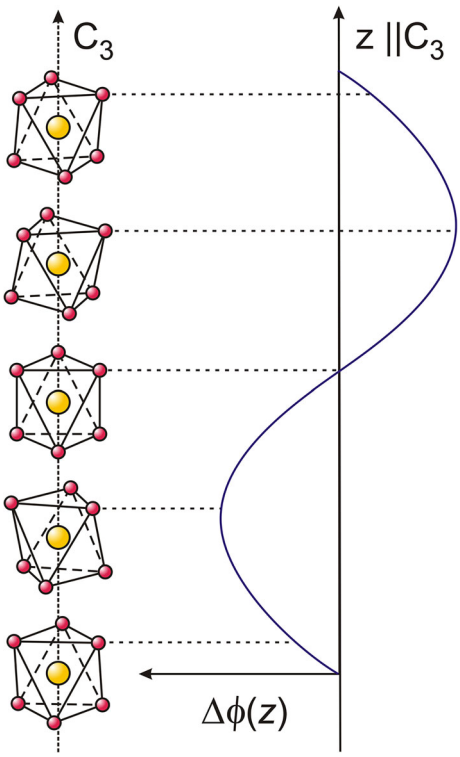

Fig. 7 Scheme of incommensurate modulation of the $[Mg(H_2O)_6]^{2+}$ (and, probably, $[SiF_6]^{2-}$) octahedra rotation $\Delta\phi$ around the direction **z** ($\|\mathbf{C}_3$) in the $MgSiF_6{\cdot}6H_2O$ crystals. The *dotted lines* show correspondence of the angles of rotation for particular octahedra to the modulation wave

with $a = 0.41$ mT and $\beta = 0.36 \pm 0.03$ (Fig. 8). It is worth noticing that calculated value of β is close to the critical exponent value in the 3d-XY Heisenberg model ($\beta = 0.345 \pm 0.002$ [35]).

In the most incommensurate systems the temperature decrease results in increase of the deviations from plane-wave approximation of modulation and the transition to non-linear so-called soliton modulation regime occurs, in which the phase function $\varphi(z)$ is determined by the solution of one-dimensional sine–Gordon equation [32]:

$$\frac{d^2\phi(z)}{dz^2} = -\alpha^2 \sin[n\phi(z)], \tag{3}$$

where $n = 2p$ [32], p unit cell multiplicity after phase transition to commensurate state, α constant determined by the soliton density n_s. In the soliton regime of modulation the decreasing soliton density n_s (at temperature decrease) is accompanied by more prominent domain-like regions of crystal with almost invariable modulation phase, which alternate with regions of sharp phase changes (similar to domain walls).

Comparison of lineshape calculations with HFS lineshapes of $MgSiF_6{\cdot}6H_2O{:}Mn^{2+}$ EPR spectra conducted for the temperature range from

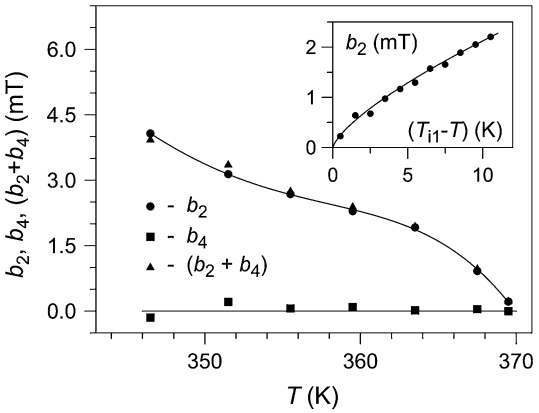

Fig. 8 Temperature dependences of incommensurate modulation parameters of the second (b_2) and fourth (b_4) order, and sum ($b_2 + b_4$) determining the effective lineshape splitting, calculated from the experimental Mn^{2+} EPR low-field HFS line for $MgSiF_6{\cdot}6H_2O{:}Mn^{2+}$ crystals for $T > T_{i2}$ (the X-band and $\boldsymbol{B}_0 \| \mathbf{C}_3$). *Solid lines* are presented as guides for the eye. In the *inset* the *dots* and *solid line* are the modulation parameter b_2 values and result of their approximation by Eq. (2)

$\approx (T_{i1} - 10$ K) to T_{i2}, in the plane-wave regime of modulation and soliton one, have demonstrated that better lineshape approximation may be reached in the soliton regime of modulation. At this regime of modulation the rather better correspondence has been reached with ($n = 6$) compared to ($n = 4$) which is seemingly expected from the data of structural investigations on doubling the crystal unit cell below T_c [8]. The reason for that may be discontinuous evolution of the distortion modulation wave in the inhomogeneous crystal phase. Indeed, according to the experimental results (Fig. 4), in the inhomogeneous phase of considered crystals the temperature dependences of the HFS lineshape parameters undergo the sequence of step-wise changes, which (taking into account the invariability of spectrum axial symmetry) may be interpreted as caused by phase transitions between states with different periods of distortion modulation (i.e., transitions between steps of the so-called "devil's staircase" [36]). Therefore, there is no reason to consider parameter n in the Eq. (3) a priori to be equal to 4 at arbitrary temperature within range of inhomogeneous phase of $MgSiF_6{\cdot}6H_2O{:}Mn^{2+}$ crystals.

Calculated dependences of the Mn^{2+} HFS lineshape parameters on angle ϕ in incommensurate phase of considered crystals, conducted with taking into account the modulation of water octahedra rotations around $\mathbf{C}_3$ axis and induced modulation of their trigonal distortions, allow to describe the principal features of respective experimental dependences (Fig. 5).

The possibility of presenting each Mn^{2+} HFS line below T_{i2} as two distinct components without spectral continuum between them (Fig. 3) indicates the abrupt decrease in amplitude of distortion modulation wave in solitons at this transition. Taking into account that below T_{i2} components of HFS lines have different temperature dependences (Fig. 2) and that only high-field component is present in the EPR spectrum of the crystals in monoclinic phase, a conclusion may be drawn that the low-field component corresponds to the soliton-like regions while the high-field

component to the domain-like ones, respectively. Qualitatively different dependences of the components of Mn^{2+} HFS lines on θ angle below T_{i2} (Fig. 6) also support this interpretation of the component origin. Indeed, the θ-dependences of high-field components of Mn^{2+} HFS lines below T_{i2} and those of Mn^{2+} HFS lines above T_{i1} are qualitatively the same and they may be simply accounted for by increase in total dipole–dipole interaction between Mn^{2+} magnetic moment and magnetic moments of 12 protons of six water molecules situated in the vertices of octahedra [37]. Narrowing the low-field component of HFS line, while θ tends to the "magic" value, is evidence that the dominant contribution to its width depends on θ as $(3\cos^2\theta - 1)$. Obviously, exactly that angular dependence is characteristic for the contribution to the inhomogeneous linewidth of component caused by the modulation of D value.

The aforementioned conception of the $MgSiF_6{\cdot}6H_2O$ crystal structure within temperature range from T_c to T_{i2} does not contradict the diffraction data as well [4, 5], having reported on the domain, commensurately modulated, structure at these temperatures. However, due to intensive dehydration of the crystals above ≈ 340 K there are no available data of X-ray diffraction on the evolution of modulated phase in the temperature range above this temperature, in particular, data on the structure transformations at T_{i2} and T_{i1}. All these considerations point out the necessity of group-theoretical (symmetry) analysis of probable paths of phase transitions in these crystals. In the following section such analysis for the phase transition at T_{i1}, possibility of structurally incommensurate states and the resulting peculiarities of the Mn^{2+} EPR spectra is presented.

5 Group-Theoretical Analysis of the Phase Transition to Structurally Incommensurate State

The presence of linear gradient terms Φ_L (so-called Lifshitz invariants [38]) in the crystal thermodynamic potential (Landau free energy) expansion on the powers of order parameter is the necessary requirement for realization of incommensurately modulated phase conditioned by fundamental symmetry reasons (so-called type-I incommensurate phase [39]). In particular case of two-component order parameter the Lifshitz invariants are antisymmetrical linear combinations as follows:

$$\Phi_L = \sigma\left[\eta_1 \frac{d\eta_2}{dz} - \eta_2 \frac{d\eta_1}{dz}\right], \tag{4}$$

where η_1 and η_2 are components of order parameter characterized by certain irreducible representation of initial space group (SG), z spatial coordinate, σ some coefficient.

The determination of the Lifshitz invariant presence for the certain system may be performed by standard methods of group-theoretical analysis of initial crystal SG and complete irreducible representation (CIR) responsible for considered second-order phase transition with using two following criteria: condition by Landau [38] and that by Michelson [40] (so-called "weak Lifshitz condition"—extension of original Lifshitz condition [38] to modulated phases).

As it was mentioned in Sect. 1, $MgSiF_6{\cdot}6H_2O$ crystals within the temperature range from T_c to T_{i2} belong to $R\bar{3}m$ [8] or $P\bar{3}$ [4, 5] SGs, at that the latter was proposed on the basis of more precise data compared to former. The results of structural investigations of the $MgSiF_6{\cdot}6D_2O$ [26, 28] and $Mg_{1-x}Fe_xSiF_6{\cdot}6D_2O$ [25, 27] crystals within that temperature range allow to assume the space group $R\bar{3}$ for them as well. According to Landau theory of the second-order phase transitions [38] there is close relation between crystal structures above transition and below it: SG of low-symmetry (low-temperature, as a rule) phase is a subgroup of the high-symmetry phase group (in particular, coincides with it for isostructural phase transition). Therefore, the $MgSiF_6{\cdot}6H_2O$ crystals above T_{i2} belong to one of three mentioned space groups, either to their supergroups (in the case of symmetry increasing) or subgroups (at lowering the symmetry). The phase transition at T_{i1} may be accompanied by further change in SG. Hence, in general case, it is necessary to consider the possibility of realizing above T_{i1} not only the subgroups and supergroups for three experimentally obtained SGs, but their subgroups and supergroups as well.

The subgroups and supergroups of $P\bar{3}$, $R\bar{3}$ and $R\bar{3}m$ SGs may be obtained from the tables [41]. According to EPR data the inversion symmetry of considered crystals is preserved within the entire temperature range of investigations, while axial symmetry is present above T_c. The former result allows to exclude non-centrosymmetric SGs from the found set of subgroups and supergroups, while the latter one allows to disregard the cubic system groups as possible supergroups. Further, taking into account the impossibility of transformation of the $MgSiF_6{\cdot}6H_2O$ crystal structure below T_{i1} into the structure of sixfold axis symmetry above that temperature by means of the infinitesimal atom displacements, the hexagonal system SGs should be excluded from the consideration. Moreover, the non-symmorphic supergroups $R\bar{3}c$, $P\bar{3}1c$ and $P\bar{3}c1$ are incompatible with microscopic $MgSiF_6{\cdot}6H_2O$ structure, as far as there are no suitable positions for oxygen and fluorine atoms in the vertices of octahedra [41]. The $P\bar{3}1m$ SG should not be considered as well as possible supergroup because the multiplicity and coordinates of magnesium and silicon atom positions are incompatible with those for $P\bar{3}$ group [41].

With respect to $R\bar{3}m$ and $P\bar{3}m1$ as candidates for SGs above T_{i1} the following elucidation should be made. The data of the $MgSiF_6{\cdot}6H_2O{:}Mn^{2+}$ crystal investigations by means of EPR point out the absence of water octahedra disorientations relative to trigonal axis above T_{i1} (Fig. 5). This result imposes restrictions on the structural organization of the crystals at these temperatures: $R\bar{3}m$ and $P\bar{3}m1$ groups, containing mirror planes, may be realized only in the case of vertices of water and fluorine octahedra situated on those mirror planes. However, such hard constraint on the crystal structure above T_{i1} (within temperature range of experiments) may be avoided with suggesting the existence of some praphase of $R\bar{3}m$ or $P\bar{3}m1$ symmetry at $T \gg T_{i1}$, which is inaccessible for study due to total dehydration of the sample. Therefore, one may consider that at T_{i1} $MgSiF_6{\cdot}6H_2O$ crystals undergo second-order phase transition characterized by CIRs of these SGs. It is worth noticing here that concept of praphase is widely used in literature at symmetry analysis of the phase transitions (e.g., [42–45]). In particular, the existence of praphase $R\bar{3}m$ was

supposed in the $FeSiF_6{\cdot}6H_2O$ crystals at higher temperature with respect to rhombohedral R$\bar{3}$ phase [45].

It follows from above that the set of groups promising for the analysis contains R$\bar{3}$, R$\bar{3}$m, P$\bar{3}$ and P$\bar{3}$m1. It is easy to see that, even if taking into account the possible change in SG (with possible absence of group-subgroup relation) at T_{i2} and T_{i1}, the requirements for inversion and trigonal symmetries restrict possible SGs with mentioned four groups.

Further, indicated promising SGs and corresponding CIRs characterized by stars $\{\boldsymbol{k}\}$ of trigonal symmetry group G_k of the wave vector $\boldsymbol{k}$:

1. R$\bar{3}$, R$\bar{3}$m: $\boldsymbol{k}(\Lambda) = \mu\ (\boldsymbol{a}^* + \boldsymbol{b}^* + \boldsymbol{c}^*)$, $\boldsymbol{k}(\Gamma) = 0$, $\boldsymbol{k}(Z) = 1/2\ (\boldsymbol{a}^* + \boldsymbol{b}^* + \boldsymbol{c}^*)$.
2. P$\bar{3}$, P$\bar{3}$m1: $\boldsymbol{k}(\Delta) = \mu\boldsymbol{c}^*$, $\boldsymbol{k}(\Gamma) = 0$, $\boldsymbol{k}(A) = 1/2\ \boldsymbol{c}^*$,

($\boldsymbol{a}^*$, $\boldsymbol{b}^*$ and $\boldsymbol{c}^*$ are the reciprocal lattice vectors for respective SGs, μ the variable parameter, $0 < |\mu| < 1/2$) have been tested on the existence of Lifshitz invariants with using the tables by Stokes et al. [46]. Symbols Λ, Γ, Z, Δ and A in the parentheses of wave vector notations correspond to the Brillouin zone points (by Bradley and Cracknell [47]). Points designated as Γ, Z and A are the so-called high-symmetry particular points (Lifshitz points) of Brillouin zone. For these points the number of degrees of freedom is zero, therefore, fulfillment of the weak Lifshitz condition leads to zero number of Lifshitz invariants too (hence, corresponding CIRs cannot lead to the symmetry conditioned incommensurate state). Violation of this condition for Γ, Z and A points (presence of the Lifshitz invariants) results in the thermodynamic potential minimum occurring in the vicinity of these special points (allowing incommensurate phase) and, taking into account the mentioned trigonal symmetry, it belongs to Λ (Δ) point. Therefore, we shall consider only CIRs corresponding to the points Λ (for R$\bar{3}$m and R$\bar{3}$) and Δ (for P$\bar{3}$m1 and P$\bar{3}$): Λ_i and Δ_i ($i = 1$–3), respectively; the indices designate small irreducible representations. Taking into account that different symmetry groups are possible above T_{i1}, the CIR symbols will be further accompanied with respective SG in the parentheses.

According to tables by Stokes et al. [46], Landau condition is satisfied for all Λ_i and Δ_i, but weak Lifshitz condition is violated for Λ_3 (R$\bar{3}$m), Δ_3 (P$\bar{3}$m1), $\Lambda_2\Lambda_3$ (R$\bar{3}$) and $\Delta_2\Delta_3$ (P$\bar{3}$) [combination of two CIR symbols into one corresponds to physical irreducible representation resulted from the direct sum of Λ_2 (Δ_2) and its complex conjugate Λ_3 (Δ_3)]. As a result, remaining CIRs are as follows: Λ_1 (R$\bar{3}$m, R$\bar{3}$) and Λ_2 (R$\bar{3}$m), Δ_1 (P$\bar{3}$m1, P$\bar{3}$) and Δ_2 (P$\bar{3}$m1), which may be responsible for the second-order transition to incommensurately modulated phase. Since all these CIRs are two-dimensional representations then phase transition order parameter is a two-component (η_1, η_2) one and Lifshitz invariant is of classical form Eq. (4).

As stated above, the presence of Lifshitz invariant is a necessary condition but not sufficient one for symmetry conditionality of the incommensurate phase realization in the certain crystal. Final conclusion on that possibility requires check on the compatibility of candidate CIR with microscopic structure of the crystal (i.e., real occupation of the crystallographic SG positions by various atoms). In terms of the representation theory it means that tensor representation (reducible, in general) built on the localized atom functions of the structure and corresponding to the nature of given phase transition (vector-type representation in the case of displacive phase

transition) should contain candidate CIR [44]. The calculations performed according to procedure stated in [44] have shown that respective tensor representations for atoms of oxygen and fluorine contain all selected CIRs, i.e., latter representations are compatible with the microstructure of the $MgSiF_6{\cdot}6H_2O$ crystals.

It is worth mentioning that tensor representations for magnesium and silicon atoms contain only $\Lambda_1(R\bar{3}m, R\bar{3})$ and $\Delta_1(P\bar{3}m1, P\bar{3})$. Therefore, for the Λ_2 $(R\bar{3}m)$ and Δ_2 $(P\bar{3}m1)$ the displacements of Mg and Si atoms are strictly zero, while for Λ_1 $(R\bar{3}m, R\bar{3})$ and Δ_1 $(P\bar{3}m1, P\bar{3})$, in general, they are distinct from zero (with preserving central positions of Mg and Si inside octahedra) and are directed along trigonal axis. The displacements of central ions (in the $P\bar{3}$ positions relative to their positions in the corresponding rhombohedral phase) were observed in the compounds $MnSiF_6{\cdot}6H_2O$ (Torii et al. [48]); however, they were not detected in $MgSiF_6{\cdot}6H_2O$ at 320 and 313 K [5, 25, 26]. For this reason, the mentioned displacements should not enter into the distortions determined by the primary order parameter.

For the case of phase transition to incommensurate state described by CIRs Λ_2 $(R\bar{3}m)$ or Δ_2 $(P\bar{3}m1)$ the basis functions of these CIRs, determining the $MgSiF_6{\cdot}6H_2O$ crystal structure transformation, have been calculated by us in the form of symmetrized displacements of oxygen and fluorine atoms (with using Kovalev tables of small irreducible representations [49]). Atoms of the same octahedron belong to two orbits with respect to symmetry elements of $G_k = 3m$ (Fig. 9) and, therefore, calculations for them have been carried out independently. The calculated atom displacements are situated in the plane being perpendicular to the trigonal axis, displacements themselves are perpendicular to radii-vectors (with respect to the centers of octahedra) of the corresponding atoms (Fig. 9). According to the aforementioned EPR results (see Sect. 3) and structure investigations data [4, 5, 8, 25] on $MgSiF_6{\cdot}6H_2O$ crystals the $[Mg(H_2O)_6]^{2+}$ and $[SiF_6]^{2-}$ octahedra possess local inversion symmetry (within entire temperature range of experiments). Consequently, the directions of atom rotations for different orbits coincide and, at

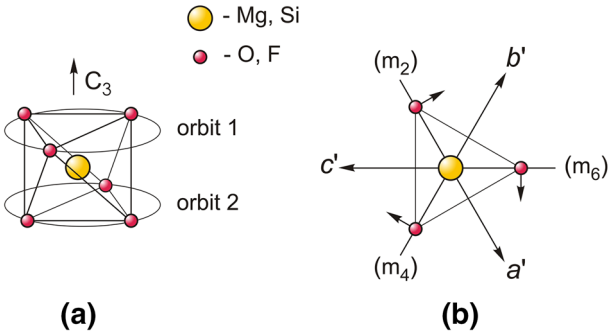

Fig. 9 Scheme of: **a** atom (O or F) distribution on the orbits for octahedron ($[Mg(H_2O)_6]^{2+}$ or $[SiF_6]^{2-}$), hydrogen atoms are not shown for clarity, **b** atomic displacements (projected onto plane being perpendicular to the $\mathbf{C}_3$ axis), corresponding to the basis functions of Λ_2 $(R\bar{3}m)$ and Δ_2 $(P\bar{3}m1)$ CIRs, for orbit 1. Symbols m_i $(i = 2, 4, 6)$ designate mirror planes (according to [49]), a', b' and c' the projections of rhombohedral lattice primitive vectors

microscopic level, phase transition at T_{i1} is determined by rotations of octahedra as a whole. Therefore, the angle of water (and/or fluorine) octahedra rotation is a primary order parameter of the phase transition to the incommensurately modulated phase. On the contrary, axial distortions of octahedra do not transform according to the mentioned CIRs and, as consequence, may be only secondary order parameters of phase transition at T_{i1}.

For $\Lambda_1(R\bar{3}m)$ and $\Delta_1(P\bar{3}m1)$ CIRs the symmetrized displacements of oxygen and fluorine atoms, forming octahedra, differ from zero and are represented with superposition of radial displacements and those along trigonal axis. The pattern of structural distortions for Λ_1 ($R\bar{3}$) and Δ_1 ($P\bar{3}$) is more complex: their basis functions contain displacements corresponding to the rotation of octahedra around trigonal axis in addition to the aforementioned displacements.

It follows from above that for the selected CIRs the primary order parameter of the phase transition at T_{i1} is determined (as magnitude of atom displacements of water and/or fluorine octahedra with respect to the high-temperature phase above T_{i1}) in the following way:

1. Λ_2 ($R\bar{3}m$) and Δ_2 ($P\bar{3}m1$)—the angle of octahedra rotation around trigonal axis (case ψ_3 according to Fig. 10).
2. Λ_1 ($R\bar{3}m$) and Δ_1 ($P\bar{3}m1$)—the magnitude of axial distortions of octahedra relative to trigonal axis (case of combination of ψ_1 and ψ_2 distortions according to Fig. 10).
3. Λ_1 ($R\bar{3}$) and Δ_1 ($P\bar{3}$)—the combination of axial distortions and rotations of octahedra around trigonal axis. The ratio between those components is determined with the parameters of interatomic interactions in studied crystals (case of combination of ψ_1, ψ_2 and ψ_3 distortions according to Fig. 10).

From these options only the first choice is in agreement with experimental data indicating that in the ferroelastic phase of $MgSiF_6{\cdot}6H_2O$ crystals there are water

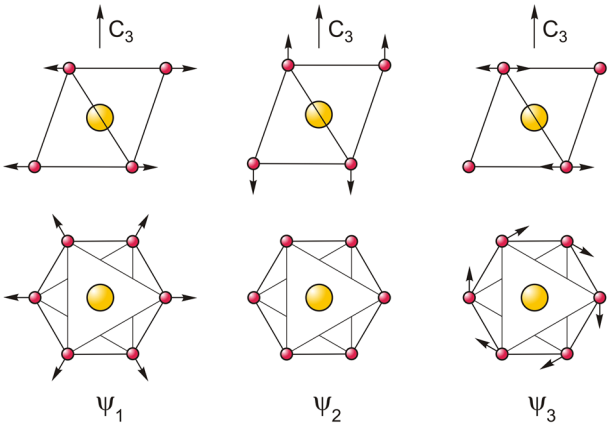

Fig. 10 Scheme of atomic displacements corresponding to the components of basis functions of CIRs: ψ_1 radial displacements, ψ_2 axial displacements along $\mathbf{C}_3$, ψ_3 rotation of octahedron around $\mathbf{C}_3$. Lateral view (*first row*) and top view (*second row*) with respect to $\mathbf{C}_3$ axis are presented. *Large circles* correspond to the Mg(Si) atoms, *small ones* to the O(F) atoms, respectively

molecule octahedra with two different orientations around trigonal axis of complexes but with equal axial distortions. Therefore, the description of the phase transition at T_{i1} with the Λ_2 ($R\bar{3}m$) or Δ_2 ($P\bar{3}m1$) CIRs and with using the concept of praphase ($R\bar{3}m$ or $P\bar{3}m1$, respectively) is the most preferable variant.

The stars of all selected CIRs consist of two arms and basis functions corresponding to arms $\boldsymbol{k}$ and $-\boldsymbol{k}$ (which are parallel to trigonal axis) depend on translation $\mathbf{z}$ as $\exp(i\boldsymbol{kz})$ and $\exp(-i\boldsymbol{kz})$, respectively [44]. In other words, order parameter components (coefficients at basis functions), determining the amplitudes of respective distortions, in the $MgSiF_6{\cdot}6H_2O$ crystals below T_{i1} are the one-dimensionally modulated ones along trigonal axis with period specified by variable parameter μ, which may take on, in general, irrational values.

The presence of variable parameter μ in the expressions for wave vector of the star for all considered CIRs means that respective non-Lifshitz point of Brillouin zone may arbitrarily move along trigonal axis within wide range without change in symmetry. Thus, at variation of external conditions the modulation wave vector may take on values being commensurate, as well as incommensurate, to the wave vector of the structure without modulation, i.e., in the $MgSiF_6{\cdot}6H_2O$ crystals at variable external parameters (e.g., temperature) it may vary in the regime of "devil's staircase" [36].

Therefore, the results of group-theoretical analysis of the phase transition in the $MgSiF_6{\cdot}6H_2O$ crystals at T_{i1} are in agreement with conclusions on the nature of inhomogeneous phase, dimensionality and direction of incommensurate modulation, order parameter of the phase transition and origin of the sequence of step-wise changes in the slopes of temperature dependences of HFS lineshape parameters in the incommensurate phase, drawn on the basis of analysis of Mn^{2+} EPR data in these crystals.

6 Conclusion

By means of EPR in the $MgSiF_6{\cdot}6H_2O{:}Mn^{2+}$ crystals at $T_{i1} = 370 \pm 0.3$ K the second-order phase transition to structurally inhomogeneous state, existing down to temperature of the improper ferroelastic phase transition at $T_c = 298.5 \pm 0.3$ K, has been investigated. The data on temperature and angular dependences of Mn^{2+} EPR spectrum and on HFS lineshapes in that phase have shown that they may be interpreted within the framework of the model of one-dimensionally modulated structurally incommensurate phase. The same data indicate that primary modulated distortion in the incommensurate phase may be the angle of $[Mg(H_2O)_6]^{2+}$ (and, probably, $[SiF_6]^{2-}$) octahedra rotation around modulation direction $\mathbf{C}_3$. As temperature decreases in the examined crystals there has been observed a gradual transformation from plane-wave distortion modulation to the non-linear soliton regime of modulation, interrupted at $T_{i2} = 343 \pm 0.3$ K by the first-order phase transition accompanied by abrupt decrease in the modulation amplitude. The group-theoretical analysis of the phase transition at T_{i1} in the $MgSiF_6{\cdot}6H_2O$ crystals has been conducted for the first time. It has shown that the crystal thermodynamic potential should contain Lifshitz invariant and, therefore, realization of the

incommensurately modulated structure is caused by fundamental symmetry reasons. The conclusions of group-theoretical study on the structure and possible character of its temperature evolution within incommensurate phase agree with the data of EPR investigations of the $MgSiF_6{\cdot}6H_2O{:}Mn^{2+}$ crystals.

Acknowledgments We thank Prof. R.L. Davidovich and Dr. T.F. Antohina for providing us with the $MgSiF_6{\cdot}6H_2O{:}Mn^{2+}$ crystals and Dr. V.G. Kuryavyi for help in the EPR experiments.

References

1. W.C. Hamilton, Acta Crystallogr. **15**, 353 (1962)
2. S. Ray, A. Zalkin, D.H. Templeton, Acta Crystallogr. B **29**, 2741 (1973)
3. D.C. Price, Can. J. Phys. **65**, 1280 (1987)
4. G. Jehanno, F. Varret, Acta Crystallogr. A **31**, 857 (1975)
5. G. Chevrier, G. Jehanno, Acta Crystallogr. A **35**, 912 (1979)
6. G. Chevrier, A. Hardy, G. Jehanno, Acta Crystallogr. A **37**, 578 (1981)
7. M. Majumdar, S.K. Datta, J. Chem. Phys. **42**, 418 (1965)
8. S. Syoyama, K. Osaki, Acta Crystallogr. B **28**, 2626 (1972)
9. Yu.V. Yablokov, M.M. Zaripov, A.M. Ziatdinov, R.L. Davidovich, Chem. Phys. Lett. **48**, 443 (1977)
10. R.S. Rubins, Kian-Kwet Kwee, J. Chem. Phys. **66**, 3948 (1977)
11. B. Ghosh, N. Chatterjee, A.N. Das, S.K. Dutta Roy, Amitava Pal, J. Phys. C Solid State Phys. **10**, L527 (1977)
12. J. Chappert, G. Jehanno, F. Varret, J. Phys. (Paris) **38**, 411 (1977)
13. T. Chattopadhyay, F. Devreux, K. Peters, E.-M. Peters, E. Gmelin, B. Ghosh, J. Phys. C Solid State Phys. **21**, 1321 (1988)
14. A.M. Ziatdinov, V.G. Kuryavyi, Ferroelectrics **143**, 99 (1993)
15. P.G. Skrylnik, A.M. Ziatdinov, Ferroelectrics **249**, 279 (2001)
16. P.G. Skrylnik, A.M. Ziatdinov, J. Phys. Condens. Matter **14**, 11671 (2002)
17. S.K. Misra, M. Kahrizi, Solid State Commun. **45**, 967 (1983)
18. I.M. Krygin, G.N. Neilo, A.D. Prokhorov, Solid State Phys. **35**, 2196 (1993)
19. A. Kassiba, R. Hrabanski, D. Bonhomme, A. Hader, J. Phys. Condens. Matter **7**, 3339 (1995)
20. K.L. Wan, S.L. Hutton, J.E. Drumheller, R.S. Rubins, J. Chem. Phys. **84**, 41 (1986)
21. K.N. Shrivastava, Chem. Phys. Lett. **20**, 106 (1973)
22. M.M. Zaripov, A.M. Ziatdinov, Yu.V. Yablokov, R.L. Davidovich, T.F. Levchishina, Sov. Phys.-Solid State **17**, 1164 (1975)
23. R.D. Weir, K.E. Halstead, L.A.K. Staveley, Faraday Discuss. Chem. Soc. **69**, 202 (1980)
24. T.G. Cherkasova, E.S. Tatarinova, E.V. Cherkasova, Russ. J. Inorg. Chem. **49**, 1064 (2004)
25. G. Chevrier, J. Solid State Chem. **111**, 322 (1994)
26. G. Chevrier, J. Solid State Chem. **99**, 276 (1992)
27. M. Hellenbrandt, Crystallogr. Rev. **10**, 17 (2004)
28. P. Villars (ed.), *Landolt-Boernstein: Crystal Structures of Inorganic Compounds*, vol. 43, Part 8 (Springer, Berlin, 2010)
29. P. Mialhe, A. Briguet, A. Erbeia, Solid State Commun. **9**, 755 (1971)
30. B. Bleaney, D.J.E. Ingram, Proc. R Soc. Lond. A **205**, 336 (1951)
31. T. Arakawa, J. Phys. Soc. Jpn. **9**, 790 (1954)
32. R. Blinc, P. Prelovsek, V. Rutar, J. Seliger, S. Zumer, in *Modern Problems in Condensed Matter Sciences*, vol. 14.1, ed. by R. Blinc, A.P. Levanyuk (North-Holland–Elsevier Science Publishers B.V, Amsterdam, 1986), pp. 143–276
33. D.J. Newman, B. Ng, Rep. Prog. Phys. **52**, 699 (1989)
34. K.A. Muller, W. Berlinger, Phys. Rev. Lett. **26**, 13 (1971)
35. J.C. Le Guillou, J. Zinn-Justin, Phys. Rev. B **21**, 3976 (1980)
36. S. Aubry, in *Solitons and Condensed Matter Physics (Solid State Sciences)*, vol. 8, ed. by A.R. Bishop, T. Schneider (Springer, New York, 1978), pp. 264–277

37. A. Abragam, B. Bleaney, *Electron Paramagnetic Resonance of Transition Ions* (Clarendon Press, Oxford, 1970)
38. L.D. Landau, E.M. Lifshitz, *Statistical Physics, Part 1 (Course of Theoretical Physics, Vol. 5)* (Pergamon Press, Oxford, 1980)
39. A.D. Bruce, R.A. Cowley, A.F. Murray, J. Phys. C Solid State Phys. **11**, 3591 (1978)
40. A. Michelson, Phys. Rev. B **18**, 459 (1978)
41. Th Hahn (ed.), *International Tables for Crystallography*, vol. A, 5th edn. (Springer, Dordrecht, 2002). (corrected reprint 2005)
42. A.P. Levanyuk, D.G. Sannikov, Sov. Phys. JETP **33**, 600 (1971)
43. K. Aizu, J. Phys. Soc. Jpn. **44**, 683 (1978)
44. Yu.A. Izyumov, V.N. Syromyatnikov, *Phase Transitions and Crystal Symmetry* (Springer, Dordrecht, 1990)
45. P. Toledano, J.-C. Toledano, Phys. Rev. B **16**, 386 (1977)
46. H.T. Stokes, D.M. Hatch, H.M. Nelson, Phys. Rev. B **47**, 9080 (1993)
47. C.J. Bradley, A.P. Cracknell, *The Mathematical Theory of Symmetry in Solids: Representation Theory for Point Groups and Space Groups* (Clarendon Press, Oxford, 1972)
48. A. Torii, K. Ogawa, H. Tamura, K. Osaki, Acta Crystallogr. C **53**, 833 (1997)
49. O.V. Kovalev, *Representations of the Crystallographic Space Groups: Irreducible Representations, Induced Representations, and Corepresentations*, 2nd edn., ed. by H.T. Stokes, D.M. Hatch (Gordon and Breach Science, London, 1993)